

DOI: 10.1002/ ((please add manuscript number))

Article type: article

Rational Design of TADF Polymers using a DA Monomer with Enhanced TADF Efficiency induced by the Energy Alignment of Charge Transfer and Local Triplet Excited States.

*Roberto S. Nobuyasu¹, Zhongjie Ren¹, Gareth C. Griffiths, Andrei S. Batsanov, Przemyslaw Data, Shouke Yan, Andrew P. Monkman, Martin R. Bryce, and Fernando B. Dias**

R. S. Nobuyasu, Dr. Przemyslaw Data, Dr. Gareth Griffiths, Prof. A.P. Monkman, Dr. Fernando B. Dias
Durham University, Physics Department, South Road, Durham, DH1 3LE, UK.
E-mail: f.m.b.dias@durham.ac.uk

Dr. Z. Ren, Dr. Andrei S. Batsanov, Prof. M. R. Bryce
Durham University, Chemistry Department, South Road, Durham, DH1 3LE, UK.

Dr. Z. Ren, Prof. S. Yan
State Key Laboratory of Chemical Resource Engineering, Beijing University of Chemical Technology, Beijing 100029, China.

Dr. Przemyslaw Data
Faculty of Chemistry, Silesian University of Technology, M. Strzody 9, 44-100 Gliwice, Poland

Keywords: TADF, Conjugated Polymers, OLEDs, Dibenzothiophene-*S,S*-dioxide; Phenothiazine

The photophysics of thermally activated delayed fluorescence (TADF) in an phenothiazine-dibenzothiophene-*S,S*-dioxide (PTZ-DBTO2) molecule is investigated in detail. We first show that the proximity of local triplet excited states (³LE), e.g. ³D or ³A, above or below the DA charge transfer states (CT) is crucial for the efficiency of the TADF mechanism in PTZ-DBTO2. This TADF emitter is then used as a monomer unit to design polymer materials with efficient TADF. The reverse intersystem crossing mechanism (RISC) that supports TADF is able to compete with internal conversion and triplet-triplet annihilation (TTA) in the polymer chains and generate efficient TADF emission in the polymer pristine films. Prototype devices with PTZ-DBTO2 dispersed in 4,4'-bis(*N*-carbazolyl)-2,2'-biphenyl (CBP) host give excellent performance with EQE of ~22% at low luminance (<100 cd/m²), for 100 cd/m² the EQE is

19.4%. In the case of solution processed devices, using the novel TADF polymers, the performance was much lower, EQE~3.5% at 100 cd/m², which is still the highest value for a polymer TADF system at useful brightness, yet reported. This results from a combination of weak charge transport properties in these materials and device fabrication methods that require further improvement. Nevertheless, these results pave the way to explore TADF in polymer light emitting diodes (PLEDs), using less costly deposition methods, such as spin-coating and inkjet printing, which are more appropriate for large area deposition.

1. Introduction

Thermally activated delayed fluorescence (TADF),¹ also known as E-type delayed fluorescence,² has very rapidly gained interest as a mechanism to improve OLED efficiencies, due to the possibility of harvesting 100% of the excitons formed by direct charge recombination, and without requiring the use of expensive and scarce metals such as iridium or platinum,³ and also avoiding the degradation issues that affect organic phosphors in the blue spectral region.⁴

TADF is also finding application in other areas, for example fluorescence-imaging due to the extended fluorescence lifetime and large Stokes shift observed in TADF materials, which allows filtering out the sample auto fluorescence and avoids scattering effects, whilst giving fluorescent probes that are not based on heavy metals.⁵ TADF is thus of general interest for any area where extending the excited state lifetime would bring significant advantages. Therefore, the TADF mechanism and possible ways to optimize material structures are of great relevance for a range of applications, including those where polymer materials might be more suitable.

The observation of efficient TADF requires the 'dark' triplet excited states to be easily harvested back to the emissive singlet manifold, using the thermal energy to assist reverse

intersystem crossing (RISC) and promote the up-conversion of lower-energy triplet states into the emissive singlet manifold. The efficiency of this mechanism is controlled by two main parameters: (i) the energy splitting between the singlet and triplet states (ΔE_{ST}), which needs to be minimized, and (ii) the suppression of non-radiative pathways available for the excited singlet and triplet states to decay, in order to obtain high fluorescence quantum yields and long triplet excited state lifetimes.⁶

To achieve a small energy splitting between the singlet and triplet excited states, as it is required to maximize triplet harvesting by reverse intersystem crossing, molecules should possess excited states of strong charge transfer character, such that the red shifted CT states lie much closer to the local triplet states of the donor or acceptor units so a small overlap can be obtained between the highest occupied and lowest unoccupied molecular orbitals, HOMO and LUMO, respectively. However, increasing the charge transfer character of the excited state leads in general to lower fluorescence yields which impact on device efficiencies.⁷ One way to solve this dilemma is to use electron-donor (D) and electron-acceptor (A) units linked in nearly-perpendicular relative orientation in the TADF emitter, and forming ‘rigid’ molecular structures, which suppresses the non-radiative decay due to the internal conversion channels.^{8,9} This arrangement is able to give fluorescence with high efficiency, while retaining negligible ΔE_{ST} , and thus achieve efficient triplet harvesting.

While great progress has been made in TADF OLEDs, particularly for emitters in the green spectral region, still major difficulties persist in the development of new molecules showing efficient TADF in the blue and red regions. Further research is thus necessary to fully understand the TADF mechanism and to facilitate new ways to design alternative molecular structures and explore alternative mechanisms.

One aspect that remains unclear is the role of spin orbit coupling (SOC) and hyperfine

coupling (HFC) in the reverse intersystem crossing mechanism. Previous work has shown that in the one-electron approximation, intersystem crossing due to spin orbit coupling between the singlet charge transfer state (^1CT) and a locally triplet excited state (^3LE) is of fundamental importance to harvest triplet states, since the interconversion between the ^1CT and ^3CT states is often not efficient.^{10,11} However, the presence of a local triplet energetically close to the CT manifold will strongly influence the efficiency of the TADF mechanism through charge transfer spin orbit coupling. Here, we explore the energy alignment between the CT manifold and a local triplet excited state in order to maximize the reverse intersystem crossing in a phenothiazine-dibenzothiophene-*S,S*-dioxide molecule, so this emitter can be used to design polymer materials showing efficient TADF emission in their pristine films.

Most TADF devices are fabricated by vacuum deposition, however solution-processing methods are also very attractive for OLEDs due to their simplicity and lower cost compared to vacuum deposition. Film deposition directly from solution, and in particular of polymers, can be used to achieve better alignment of the chains, thus increasing charge mobility and potentially enhancing device efficiencies due to better light extraction.¹² However, while TADF OLEDs fabricated from solution have been reported recently with a small-molecule emitter dispersed in diphenyldi(4-(9-carbazolyl)phenyl)silane host,¹³ to date TADF has been very rarely observed in conjugated oligomers and polymers.

Small molecule films deposited from solution usually suffer from poor quality, and the advantages offered by solution processing methods, such as spin-coating, spray-on and ink-jet printing, which allow rapid deposition over large areas at room temperature, and using large flexible substrates,¹² are still largely unavailable for TADF devices. Further work is thus necessary to investigate ways to promote efficient TADF in large molecules that are more suitable for solution processed devices.

Two factors explain why the observation of TADF is challenging in oligomers and polymers. First, simultaneously achieving small ΔE_{ST} and suppressing internal conversion is very difficult in molecules containing many atoms. Secondly, intramolecular and intermolecular triplet-triplet annihilation (TTA) is often operative and efficiently quenches the triplet population in polymers and oligomers.¹⁴ Indeed, it is mainly to avoid TTA that small TADF molecules are dispersed in hosts with high triplet energy levels.

Unfortunately, host molecules often adversely influence the photoluminescence (PL) and electroluminescence (EL) properties of TADF emitters, causing large variations in the emission yield and lifetime due to host-guest exciplex formation,¹⁵ and heterogeneities in the host-guest molecular geometries.¹⁶ Host-guest systems are also susceptible to phase separation due to the differences between the molecular structures of the constituent molecules, which may result in unstable luminescence. Therefore, achieving efficient TADF in pristine materials, i.e. without using host-guest systems, is of major interest and has only very recently been reported.¹⁷

During the preparation of this manuscript Albrecht *et al*¹⁸ reported TADF in films of a solution-processable, non-doped, dendrimer; however, the dendritic structure is clearly distinct from the polymers described here. More recently and in parallel with our work, Nikolaenko *et al.*¹⁹ reported TADF in a linear polymer, but structurally different from our polymers. The EQE reported in Nikolaenko's work is around 10%, but this is only at a current density of 0.01 mA/cm² and giving ~ 2 cd/m², which is very low and not suitable for normal device operation. However, at higher current densities, 10 mA/cm², the EQE is around 3%.

2. Results and Discussion.

2.1 Photophysics. A TADF emitter, identified as PTZ-DBTO2, based on a phenothiazine donor (D) and a dibenzothiophene-*S,S*-dioxide acceptor (A), **Figure 1a**, covalently linked in

near perpendicular orientation was synthesized (see S1 in supporting information) and its structure confirmed by single-crystal X-ray analysis (see Figure S2A in supporting information). This molecule was functionalized (see supporting information for synthetic details) to provide a monomer unit to incorporate into two co-polymers, COPO1 and COPO2, which are shown to exhibit efficient TADF in their pristine films. **Figures 1b and 1c** show the absorption and emission spectra of the individual D and A fragments and of PTZ-DBTO2, all in dilute toluene solution. **Figure 1d** shows the absorption and steady-state emission spectra of COPO1 and COPO2 in their pristine films.

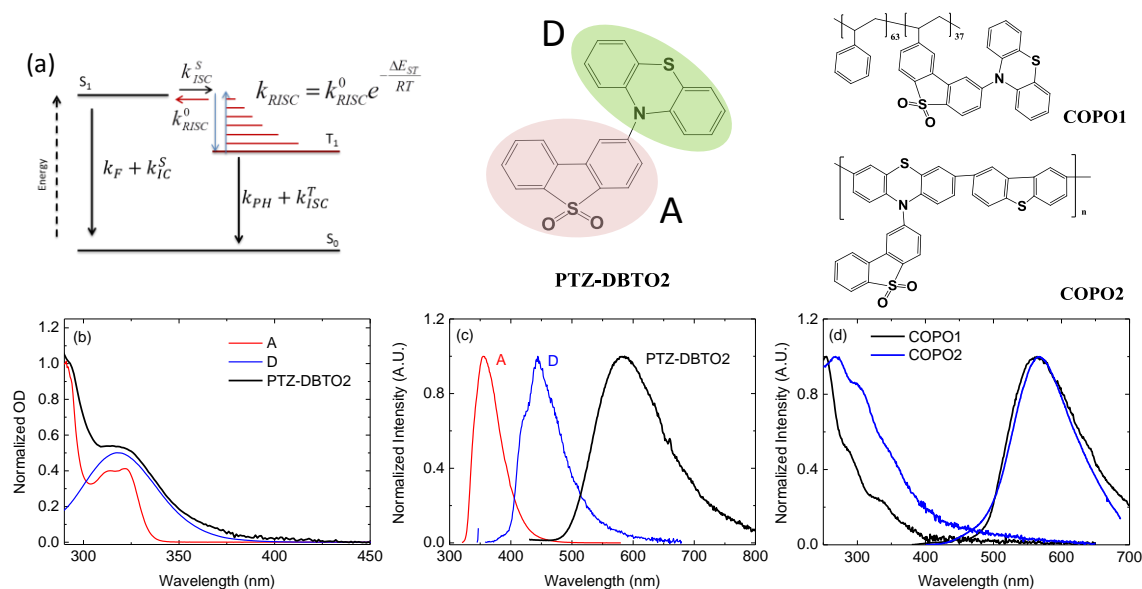


Figure 1-(a) TADF kinetic scheme, chemical structures of PTZ-DBTO2, and of copolymers COPO1 and COPO2. The electron donor (D) and electron acceptor (A) units are identified on the PTZ-DBTO2 structure. (b) Absorption spectra of the D, A fragments and of PTZ-DBTO2 in dilute toluene solution. (c) Fluorescence spectra of the D, A fragments and of PTZ-DBTO2 in toluene solution. (d) Absorption and steady-state emission spectra of COPO1 and COPO2 in their pristine films.

The HOMO-LUMO levels of PTZ-DBTO2, -5.4 eV and -2.95 eV, respectively, and of the two copolymers, COPO1, -5.35 eV and -2.9 eV, and COPO2, -5.3 eV and -3.0 eV, were determined by electrochemistry from the CV data analysis and taking into consideration that

the EA and IP directly correspond to the LUMO and HOMO energies respectively, see Figure S4 in supporting information.

The data established that the amphoteric redox behavior of the DA unit, PTZ-DBTO2, is retained in the two copolymers, and in general the copolymers and PTZ-DBTO2 have a very similar oxidation potential, with COPO2 showing slightly lower oxidation onset potential, which is consistent with the increased conjugation length compared to COPO1. A larger difference is observed in the reduction part of the CV: COPO1 is slightly more difficult to reduce than both COPO2 and PTZ-DBTO2. This is possibly due to steric effects which make it more difficult to flatten the COPO1 structure during the doping process.

Consistent with the single-crystal X-ray data and calculations, the absorption spectrum of PTZ-DBTO2 is almost entirely formed by the superposition of the D and A absorptions (Figure 1b). This is due to the very limited conjugation between the D and A units, which is imposed by the nearly perpendicular D-A orientation.

The fluorescence from PTZ-DBTO2 appears broad and featureless, independently of the polarity of the medium in which the PTZ-DBTO2 is dissolved, and is red-shifted from the D and A emissions, which in toluene peak at 356 nm (A) and 445 nm (D), giving indication for strong charge transfer character of the excited state in both solution and solid state.²⁰ The Stokes-shift is large, and the emission peaks between 540 nm and 600 nm depending on the solvent polarity (Figure 1c). The emissive singlet state in PTZ-DBTO2 is hereafter identified as ¹CT.

Direct population of the ¹CT state is obtained by excitation at the PTZ-DBTO2 absorption edge, where a weak $S_0 \rightarrow ^1\text{CT}$ absorption band ($\epsilon \approx 10^2 \text{ M}^{-1}\text{cm}^{-1}$) is observed at high concentrations extending up to 440 nm, (Figure S5 in supporting information).

Very efficient DF is observed from PTZ-DBTO2 in zeonex at room temperature, **Figure 2a**.

The nearly-perpendicular D-A orientation and strong CT character of the excited state gives rise to an extremely small overlap integral between the HOMO and LUMO orbitals (Figure

S3 in supporting information). This results in a very small singlet-triplet energy splitting between the lowest excited states in PTZ-DBTO2, ^1CT and ^3LE respectively, which facilitates thermally activated reverse intersystem crossing. The presence of a ^3CT state could not be inferred from our spectroscopy data. However, due to the extremely small overlap between the HOMO and LUMO orbitals in PTZ-DBTO2, the singlet and triplet CT states, ^1CT and ^3CT , should be practically degenerate.

The energy of the singlet ^1CT in zeonex is determined at RT from the onset of the DF time resolved spectra at 2.66 eV. At low temperatures however, the onset of ^1CT emission spectrum slightly contracts and the ^1CT energy is determined at 2.61 eV. The ^1CT energy is therefore between 2.61 and 2.66 eV. At early times, emission from a local excited state ^1LE , carrying contributions from ^1D and ^1A emission, is also observed. The near perpendicular arrangement between the D and A molecular units causes very low electronic coupling between them and so greatly slows down the D-A electron transfer step. Direct recombination from the ^1LE singlet state is thus able to compete with the population of the ^1CT state.

The phosphorescence spectra of the individual D and A fragments and of PTZ-DBTO2 are compared in zeonex matrix at 77 K in **Figure 2b**. At this low temperature the DF is sufficiently weak and phosphorescence from PTZ-DBTO2 is easily observed. Interestingly the PTZ-DBTO2 phosphorescence from the ^3LE state carries clear, distinct signatures from both D and A units. A higher energy triplet state, centered in the acceptor unit (^3A), is clearly observed at 2.66 eV, and a lower energy triplet state of the donor unit (^3D), emits at 2.48 eV, 0.18 eV below ^1CT . The energy of the ^3LE state is thus determined from the first vibrational at 2.66 eV, giving an energy difference between ^1CT and ^3LE of less than 0.05 eV, in excellent agreement with singlet-triplet gap of 0.0074 eV, determined from calculations, Figure S3 in the supporting information. The small energy difference between ^1CT and ^3LE explains, therefore, the efficient DF that is observed in PTZ-DBTO2. In **figure 2c** emission from the ^1CT state and phosphorescence in PTZ-DBTO2 are compared at 77 K. Note that at

low temperature the ^1CT state appears below the ^3LE , with an energy difference of 0.05 eV. However, with increasing temperature the onset of the ^1CT slightly expands, which reflects the change on the Boltzmann distribution of the ^1CT state, and the energy gap between ^3LE and ^1CT decreases, which originates enhanced TADF at higher temperatures.

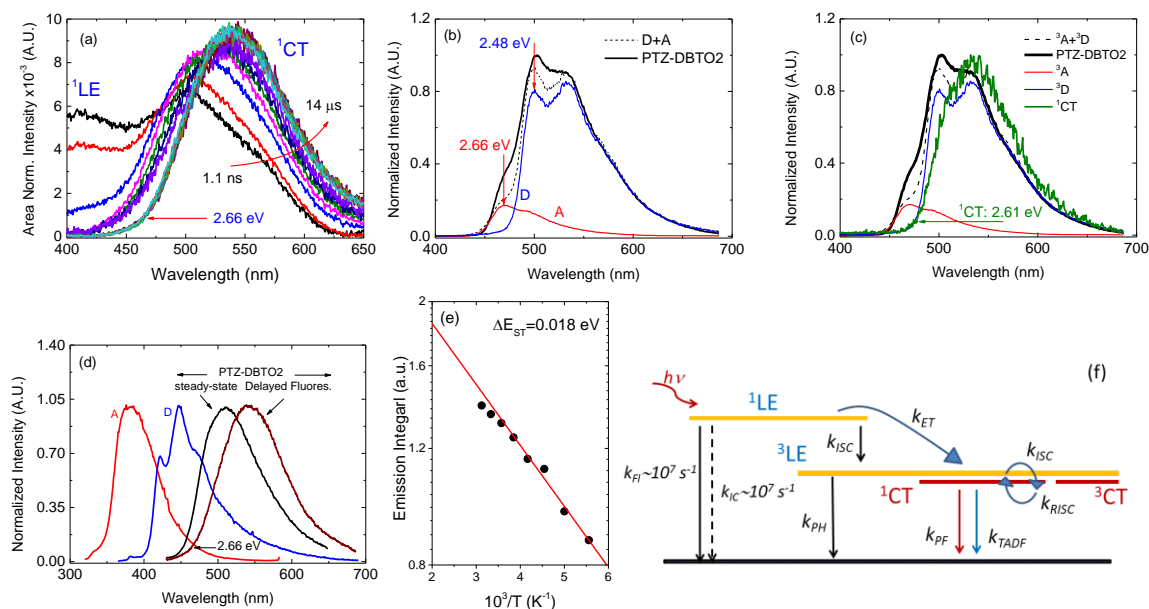


Figure 2-(a) Time resolved, area normalized, emission spectra of PTZ-DBTO2. (b) Phosphorescence of PTZ-DBTO2, compared with the phosphorescence of the isolated D and A fragments, all in zeonex at 77 K. (c) Phosphorescence of PTZ-DBTO2 compared with the ^1CT emission at 77 K in zeonex. (d) Steady-state emission spectra of the single D, A fragments and of PTZ-DBTO2, compared with the PTZ-DBTO2 delayed fluorescence. The delayed fluorescence spectrum is collected at 1 μs delay time, and integrated over 20 μs . (e) Energy barrier for TADF, determined from the temperature variation of the steady-state ^1CT emission. (f) Energy level diagram showing the electronic excited states in PTZ-DBTO2 and the main interconversion deactivation rates. All spectra, with exception of the phosphorescence, were collected in zeonex rigid matrix at room temperature.

In **Figure 2d**, the steady-state fluorescence from the individual D (peak at 448 nm), and A (peak at 381 nm) fragments and of PTZ-DBTO2 are compared with the PTZ-DBTO2 delayed fluorescence (DF) obtained in rigid zeonex matrix at room temperature. The steady state emission of PTZ-DBTO2 appears blue-shifted relative to the delayed fluorescence (DF). This is due to the contributions of residual ^1LE fluorescence, and of ^1CT spectral relaxation observed in figure 2a, which is integrated in the steady-state. The energy of the ^1CT state

determined from the integrated time resolved DF spectrum, agrees well with the previous determination, giving the ^1CT energy at 2.66 eV. The energy barrier for the observation of delayed fluorescence is determined in **Figure 2e**, using the temperature dependence of the ^1CT steady-state emission shown in **Figure 3a**. The energy barrier of ~ 0.02 eV is in excellent agreement with the expected energy difference between the ^1CT and ^3LE . This once more indicates that the strong spin orbit coupling between the ^1CT manifold and the ^3LE local triplet state explains the strong TADF that is observed in PTZ-DBTO2. Finally, in **Figure 2f** the energy level diagram and summary of the photophysical behavior in PTZ-DBTO2 is given. The main conclusion to take from figure 2 is that the ^1CT and the ^3LE states appear almost degenerate, and this gives rise to strong TADF in PTZ-DBTO2 due to the enhanced spin orbit coupling between the CT manifold and the local triplet state.

Steady-state fluorescence of PTZ-DBTO2 in zeonex as a function of temperature is shown in **Figure 3**. Between 320 K and 180 K, the PTZ-DBTO2 fluorescence is dominated by ^1LE and ^1CT emissions, peaking at 396 nm and 510 nm, respectively, **Figure 3a**. A clear isoemissive point is observed between the ^1LE and ^1CT emissions, with the intensity of the ^1CT emission decreasing when the temperature decreases, and the ^1LE emission showing the opposite trend, **Figure 3b**. This confirms that the ^1LE and ^1CT states are kinetically linked species. Finally, below 180 K, ^3LE phosphorescence emerges and dominates the emission spectra.

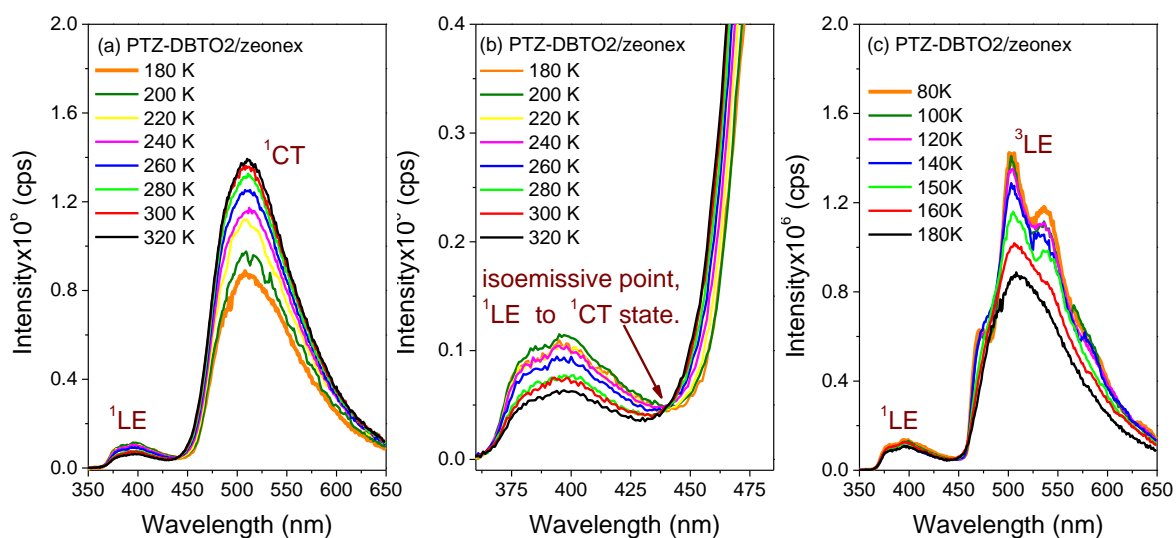


Figure 3- (a) PTZ-DBTO2 steady-state fluorescence in zeonex, from 320 K to 180 K. ^1LE and ^1CT emissions are observed. (b) A clear isoemissive point is observed between the ^1LE and ^1CT emissions. (c) PTZ-DBTO2 steady-state luminescence in zeonex, from 180 K to 80 K. ^1LE fluorescence and ^3LE phosphorescence are observed.

The PTZ-DBTO2 fluorescence decay in zeonex at room temperature is followed over a time interval covering 6 decades, see **Figure 4a**. Prompt (PF) and delayed fluorescence (DF) components are clearly observed, and both PF and DF components can only be fitted with the sums of two exponentials; a single exponential fitting of the PF decay region is also shown in red. **Figure 4b** shows the excitation power dependence of the delayed fluorescence in PTZ-DBTO2 dispersed in zeonex matrix at room temperature. The integral of the delayed fluorescence, collected with 1 μs delay time, and integrated over 100 μs , shows a perfect linear dependence with excitation power (gradient 1), showing that the origin of DF in PTZ-DBTO2 is entirely due to a monomolecular process.²¹ Finally, in **Figure 4c**, the fluorescence decay of PTZ-DBTO2 in zeonex is followed as a function of temperature. The PF shows almost no variation with temperature, consistent with negligible internal conversion (IC). However, the DF component shows clear temperature dependence, decreasing in intensity at

low temperatures, obeying an Arrhenius law, used to describe the reverse intersystem crossing rate. The DF is thus unambiguously assigned to a TADF mechanism. At low temperatures and long delay times the slower decay of phosphorescence is also observed.

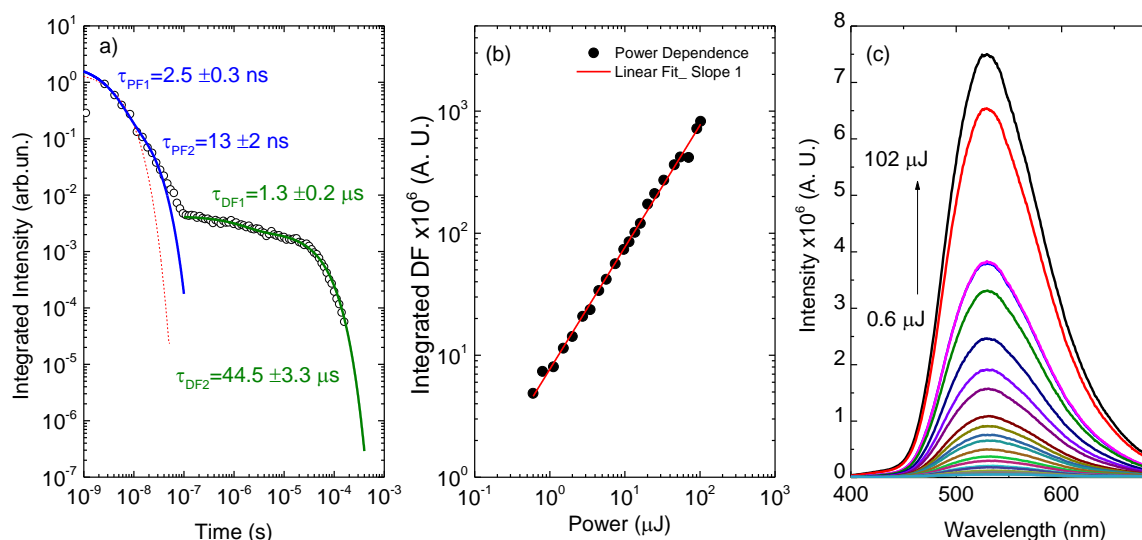


Figure 4-(a) PTZ-DBTO2 fluorescence decay, collected in zeonex at room temperature. (b) DF linear dependence with excitation power. (c) Temperature dependence of PTZ-DBTO2 fluorescence decays.

Previously, it was assumed that the TADF harvesting step involved RISC and ISC between the singlet and triplet CT states.¹ However, this process is formerly forbidden for perpendicular HOMO and LUMO orbitals, which is the case in PTZ-DBTO2, due to unfavourable spin-orbit coupling (SOC) and Franck-Condon factors.^{10,11,23} However, crossing between the ¹CT state and an energetically close local triplet state is efficient, as was shown by Dance et al.²⁴ Hyperfine coupling (HFC) can in principle interconvert ¹CT to ³CT and back.^{25,26} However the exchange energy, i.e. approximately the energy difference between ¹CT and ³CT states, would need to be smaller than the typical hyperfine energy of a large organic system, typically 20 μeV, which makes HFC rather inefficient in most systems.

Therefore in PTZ-DBTO₂, the near degeneracy of the CT manifold and the local triplet state is crucial to promote enhanced ISC due to charge transfer spin orbit coupling, and given the very small energy gap between ³LE and ¹CT, this is also ideal for thermally activated RISC.

The importance of the energy alignment between the CT manifold and ³LE triplet state can be easily tested by looking at the TADF efficiency in solvents of increasing polarity, which shifts the ¹CT state to lower energies without significantly affecting the ³LE energy, since this state has negligible dipole moment. This is shown and summarized in **Figure 5**.

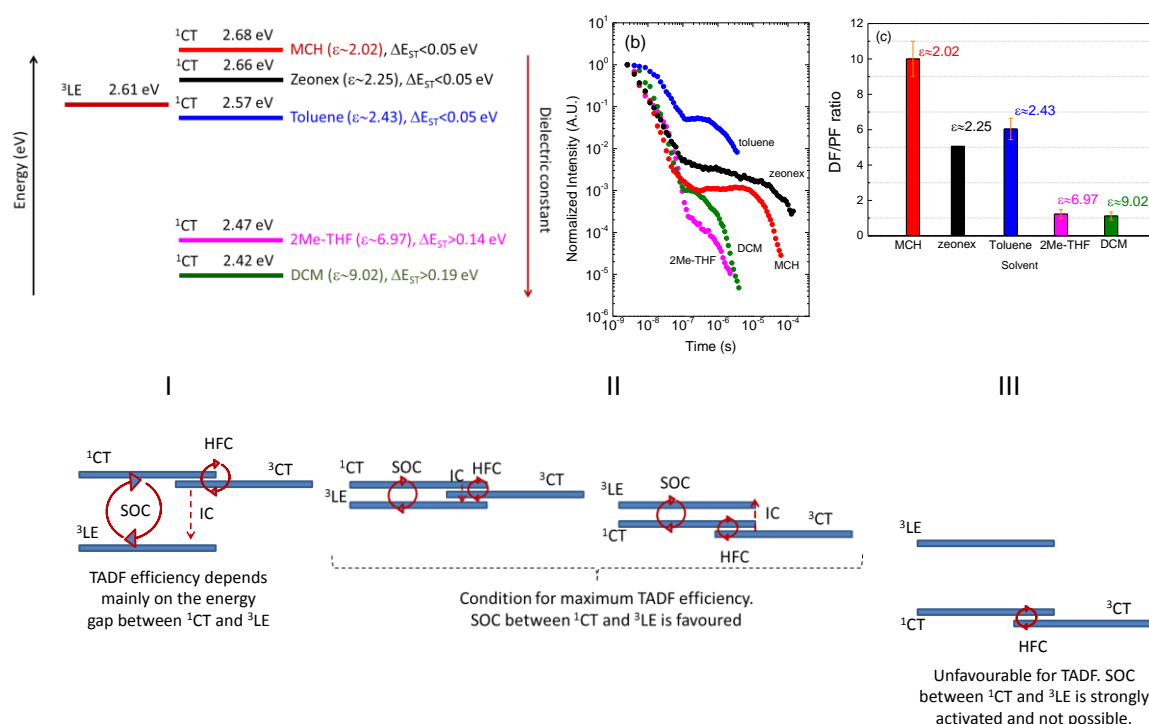


Figure 5-TOP: Influence of solvent polarity on the contribution of TADF to the PTZ-DBTO₂ fluorescence at room temperature. (a) Energy of the ¹CT state with increasing solvent polarity; (b) Time resolved fluorescence obtained in solvents of increasing polarity; (c) Emission ratio between the delayed and prompt fluorescence determined from steady-state spectra obtained in degassed and aerated conditions. BOTTOM: Diagram showing three possible situations for TADF in DA molecules with different energy ordering of their electronic excited states.

Given the favorable conditions for reverse intersystem crossing and enhanced TADF in PTZ-DBTO2, induced by the close energetic proximity of the CT manifold and the local triplet excited state in most hosts used in devices, PTZ-DBTO2 was selected as the monomer unit to design polymer materials showing efficient TADF emission.

The observation of strong TADF, as it occurs in PTZ-DBTO2, requires the following conditions to be valid (see Figure 1a): $k_{ISC}^S \gg k_F + k_{IC}^S$ and $k_{RISC} \gg k_{PH} + k_{ISC}^T$, i.e. in the S_1 state the intersystem crossing (k_{ISC}^S) dominates over the fluorescence emission (k_F) and internal conversion (k_{IC}^S), and in the T_1 state the reverse intersystem crossing (k_{RISC}) dominates over the phosphorescence emission (k_{PH}) and internal conversion (k_{IC}^T). When these conditions are met, the triplet states are recycled a number of times between the S_1 and T_1 states before giving rise to DF from S_1 .⁶

While such conditions are easily met in small molecules because the triplet states are more easily confined in the emitter, in large molecules the quenching of the triplet population due to triplet-triplet annihilation (TTA) and other non-radiative processes is very efficient because the polymer can accommodate multiple excitations enabling intrachain TTA for example,²⁷ and tuning the photophysics of the monomer unit is of fundamental importance to achieve efficient TADF emission in these materials.

PTZ-DBTO2 was used to design two copolymers, COPO1, containing PTZ-DBTO2 as a pendant group, and COPO2 with the donor phenothiazine in the polymer backbone, but separated with a dibenzothiophene spacer with a larger energy gap. In both cases the strategy is to confine the excitons in the PTZ-DBTO2 monomer. Notably, both polymers show TADF in pristine film, i.e. without using high triplet host materials to confine the triplet states in the TADF emitter, and demonstrating that in tailored polymers reverse intersystem crossing is able to compete with TTA and internal conversion, even without using high triplet hosts to disperse the TADF emitter.

The absorption of COPO1 and COPO2 in their pristine films is shown in Figure 1d in excellent agreement with the absorption of the monomer unit. However, both polymers show their absorption slightly red-shifted relative to the absorption of the monomer PTZ-DBTO2. This is particularly evident for COPO2, which is more conjugated. The emission spectra in both copolymers overlap with each other and also match with the emission of PTZ-DBTO2, both peaking at 565 nm.

The fluorescence decay of COPO1 in pristine thin film is shown in **Figure 6a**. As for the monomer PTZ-DBTO2, two decay regimes are clearly identified. A fast decay region, fitted with two exponentials, 3.85 ns and 23.5 ns, is assigned to the PF (prompt CT emission) component. This is followed by a slower decay, assigned to DF, which also shows complex decay dynamics, with three time constants, 111 ns, 0.9 μ s and 2.1 μ s. The DF contribution to the overall emission in COPO1 is calculated as 45%. **Figures 6b** and **6c** show the DF dependence with excitation dose obtained in COPO1 at room temperature, and the dependence with temperature of the COPO1 fluorescence decay, respectively. The integrated delayed fluorescence is collected with 1 μ s delay time, and integrated over 100 μ s, showing perfect linear dependence with excitation dose (gradient 1). The DF thus originates from an monomolecular process.^{20,21} Moreover, while the PF component shows no variation with temperature, suggesting negligible internal conversion (IC), as in the case of PTZ-DBTO2, the DF component clearly decreases with temperature. The DF in COPO1 is thus assigned to a TADF mechanism. The threshold delay time at which TADF significantly deviates from the PF decay also increases with decreasing temperature, and we also see the TADF lifetime increasing with decreasing temperature; both observations are consistent with a longer triplet lifetime due to a slower reverse intersystem crossing rate at lower temperatures.

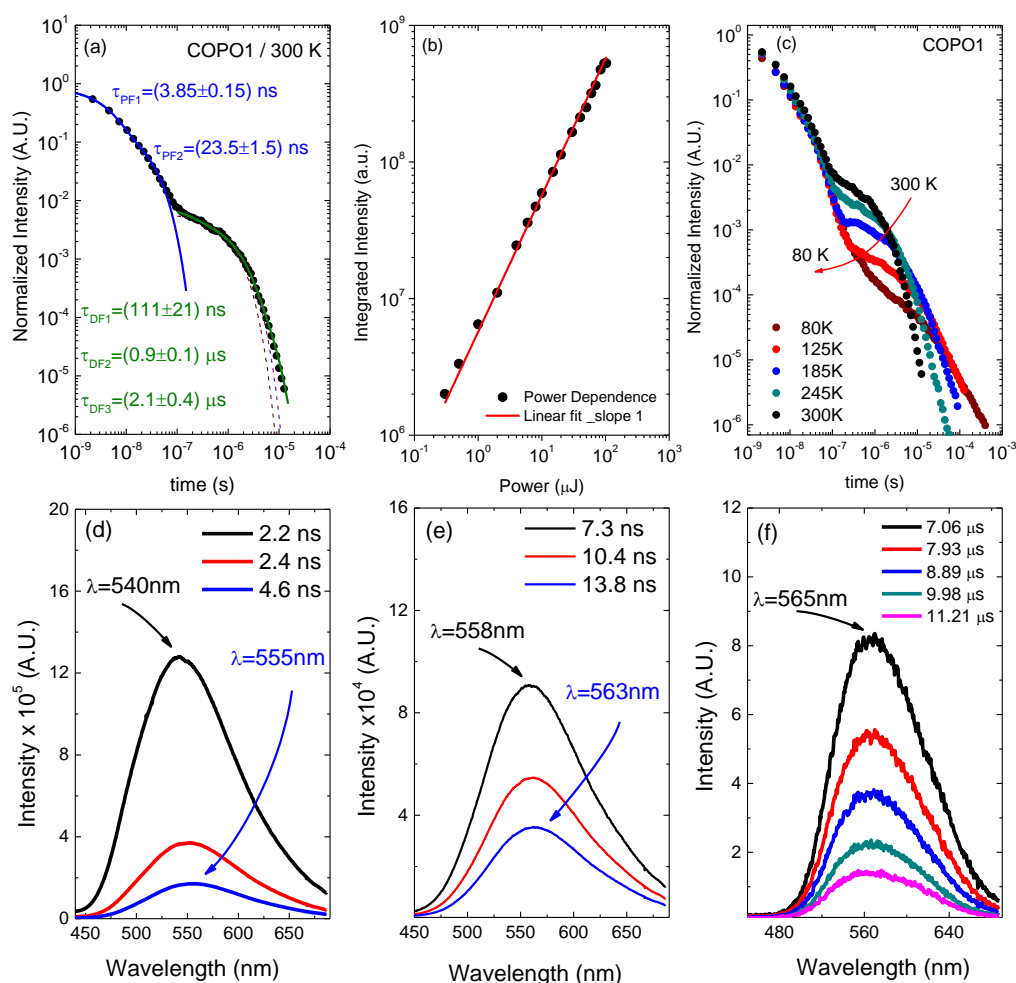


Figure 6-(a) COPO1 fluorescence decay, collected in pristine thin film at room temperature. Prompt (PF) and delayed (TADF) fluorescence components are clearly observed. Single and double exponential fits to the TADF component are shown in dark red. A perfect fit is only obtained with three exponentials. (b) TADF linear dependence with excitation power. (c) Temperature dependence of COPO1 fluorescence decays. (d-f) Time resolved fluorescence spectra of COPO1 pristine films at room temperature.

The excited state dynamics observed in PTZ-DBTO2 at early times, is much less pronounced in COPO1 films. In this copolymer only a small red shift is observed at very early times in the ^1CT emission band, but no other spectral relaxation is observed after ~ 15 ns, i.e. no deviation from the normal ^1CT emission intensity decay is observed in the time resolved spectra. However, the ^1CT emission observed at later times shows pronounced spectral narrowing, with the emission onset shifting from 475 nm at early times to 502 nm in the μs time range,

see **Figures 6d-6f**. The ^1CT energy is thus determined from the time resolved spectra obtained in the μs time domain, where pure ^1CT emission is observed, and in COPO1 appears at 2.47 eV.

With decreasing temperature the fluorescence decays in the TADF region of COPO1 become increasingly more complex, and the three exponential fit observed at room temperature is inadequate to fit the entire decay, **Figure 6c**. This is probably due to a number of reasons which can cause the decays to become more complex at low temperatures, including an increasing contribution from long-lived ^3LE phosphorescence, increasing TTA, and film heterogeneity.

The excited state dynamics in COPO2 is more pronounced than in COPO1, see figure 7.

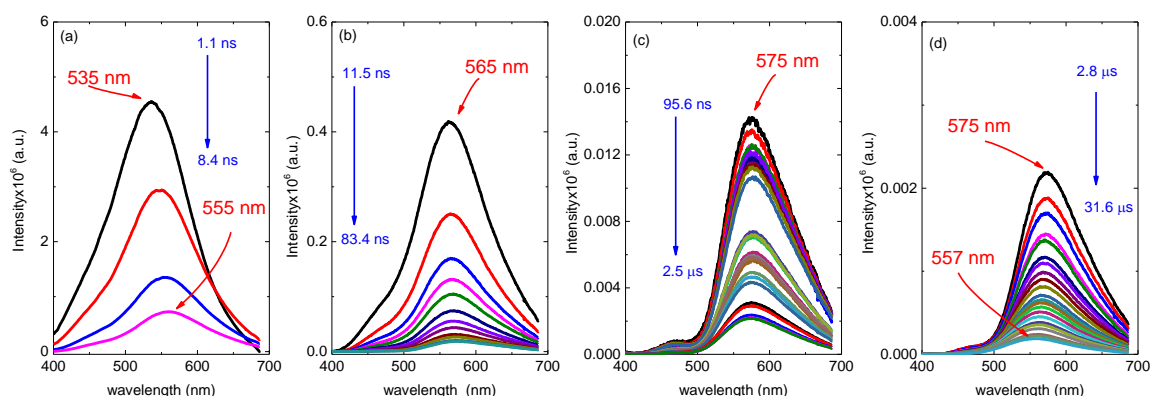


Figure 7- Time resolved fluorescence spectra of COPO2 pristine films at room temperature.

At early times the fluorescence emission of COPO2 peaks at 535 nm, but rapidly shifts to lower energies, peaking at 555 nm at 8.4 ns, 565 nm at 11.5 ns, and 575 nm from 100 ns to 2.8 μs . It then shifts back to shorter wavelengths, peaking at 577 nm at 31.6 μs . This behavior is due to a stronger energetic relaxation in the ^1CT emission and probably due to underlying phosphorescence, which becomes increasingly important when the DF becomes weaker. The energy of the ^1CT state is determined in COPO2 at 2.43 eV, using the time resolved spectra

around $2\mu\text{s}$, in order to avoid the influence of spectral relaxation and underlying phosphorescence.

Consistent with more pronounced spectral dynamics in COPO2, the fluorescence decays obtained at room temperature show a very complex behavior, see **figure 8**, and even a three exponential fit is not appropriate to fit the decays in the DF region. However, the PF still decays with a bi-exponential profile with time constants similar to those observed in COPO1, 3.4 ns and 29 ns. In the DF region the decay appears more complex, showing a long lived component that extends into the ms time range, and cannot be entirely fitted even by a sum of three exponential functions. As for COPO1, the integrated delayed fluorescence in the COPO2 pristine film, collected with $1\mu\text{s}$ delay time and integrated over $100\mu\text{s}$, shows a perfect linear dependence with excitation power (gradient 1), which clearly identifies the origin of DF in COPO2 to a monomolecular process, i.e. intersystem crossing. The fluorescence decay in COPO2 films, obtained as a function of temperature is also shown in figure 8. As in previous cases, the PF component shows no variation with temperature, while the DF component decreases as expected at low temperatures, showing that the DF in COPO2 is also due to TADF.

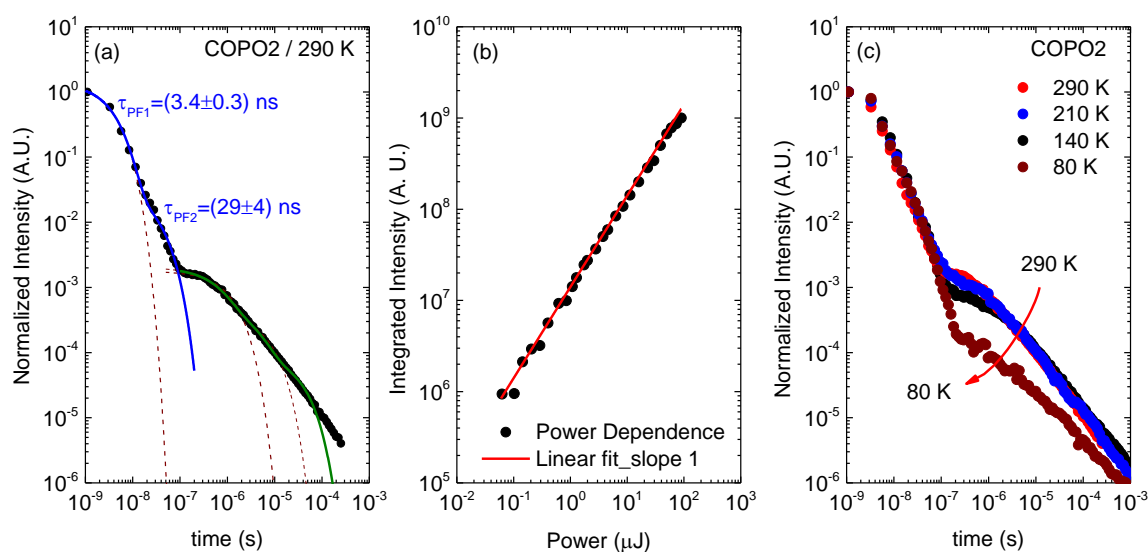


Figure 8-(a) COPO2 fluorescence decay, collected in pristine thin film at room temperature. Prompt (PF) and delayed (DF) fluorescence components are clearly observed. A perfect fit for the PF component is obtained with two exponentials. Exponential fits with one (PF), and two (DF) exponentials are also shown in dark red. (b) DF linear dependence with excitation power. (c) Temperature dependence of COPO2 fluorescence decays.

The phosphorescence spectra of PTZ-DBTO2, COPO1 and COPO2 obtained in zeonex at 80 K are compared in figure S6 in the supplementary information. Both COPO1 and COPO2 show clear phosphorescence a local triplet excited state, ^3LE , as it occurs in PTZ-DBTO2. However, while for COPO1 the phosphorescence is very similar to that observed in PTZ-DBTO2 in COPO2 the phosphorescence appears slightly broader and red shifted due to the effect of increased conjugation. This is not surprising since in COPO1 the emitter is used as a pendant group, while in COPO2 is part of the main chain, and so is more affected by conjugation.

2.2. Device fabrication and characterization. The performance of prototype devices is shown in **Figure 9**. Devices containing PTZ-DBTO2 as the emitter in CBP host (DEV1), (architecture: ITO/NPB(40 nm)/10% PTZ-DBTO2:CBP (20 nm)/TPBi (50 nm)/LiF(1 nm)/Al(100 nm), give excellent performance with EQE of ~22%, at low luminance (<100 cd/m²), for 100 cd/m² the EQE drops slightly to 19.4%. In contrast with the device made of PTZ-DBTO2 dispersed in CBP, the device with a pure PTZ-DBTO2 layer (DEV2) has much lower efficiency (ca. 3%). Here, the lower efficiency is mainly due to the low charge mobility in the emissive layer and possibly to the effect of TTA due to less triplet confinement in the pure PTZ-DBTO2 film.

Also in clear contrast with the PTZ-DBTO2:CBP devices is the performance of the solution processed polymer devices. This was expected since devices fabricated from solution often show lower performances. Moreover, we have not used any additional hole/electron

transport/blocking layers in these devices, which can contribute to explaining their weaker performance. Due to the different nature of the molecules (small molecules and polymers) we compared evaporated devices based on small molecules and spin coated devices based on polymer active layers. OLED devices were fabricated by evaporation based on mixed (DEV1) and pure (DEV2) PTZ-DBTO2 layers as emitting layers: ITO/NPB (40 nm)/10% PTZ-DBTO2 in CBP (20 nm)/TPBi (50 nm)/LiF (1 nm)/Al (100 nm) as DEV1 and ITO/NPB (40 nm)/PTZ-DBTO2 (20 nm)/TPBi (50 nm)/LiF (1 nm)/Al (100 nm) as DEV2. The polymeric derivatives of PTZ-DBTO2 were solution processed to form ITO/PEDOT:PSS (40 nm)/10% COPO1 in CBP (25 nm)/TPBi (50 nm)/LiF(1 nm)/Al (100 nm) as DEV3 and ITO/PEDOT:PSS (40 nm)/10% COPO2, 40% PBD in PVK(25 nm)/TPBi (50 nm)/LiF(1 nm)/Al (100 nm) as DEV4. The highest EQE was obtained for DEV1 around 22% but at low luminance ($<100 \text{ cd/m}^2$), for 100 cd/m^2 EQE was 19.4%. The device with a pure PTZ-DBTO2 layer (DEV2) showed much lower efficiency (ca. 3%), although the same emissive material is used. The lower efficiency is mainly due to the low charge mobilities in the emissive layer which has less effect in a doped layer. In a host-dopant emissive layer, the mobility is dependent mainly on the mobility of the host rather than the main emitter. The highest luminance was obtained for DEV1 above 15000 cd/m^2 at 13.5 V. The polymer based devices were less stable with high roll-off behaviour. The highest efficiency was obtained for COPO1 (DEV3) derivative, 2.3% at 7 V. The COPO2 based device (DEV4) achieved 11.05% at 5.5 V. The highest device efficiency was observed for DEV1 above 30 cd/A between 4-9 V. The EQE of our devices is, therefore, better than the performance recently reported in Nikolaenko's paper¹⁹ at the same brightness, 100 cd/m^2 .

Device	Luminance (cd m ⁻²)	Voltage (V)	EQE (%)	Luminous power efficiency (lm W ⁻¹)	Current efficiency (cd A ⁻¹)
DEV1	100	6.5	19.4	13.9	32.0
DEV1	1000	9.2	13.8	8.9	27.5
DEV2	100	8.1	3.1	2.3	6.1
DEV2	1000	-	-	-	-
DEV3	100	5.5	1.4	1.9	4.5
DEV3	1000	7.5	2.1	2.5	6.3
DEV4	100	7.8	3.5	3.9	10.0
DEV4	1000	11.5	2.1	1.5	5.7

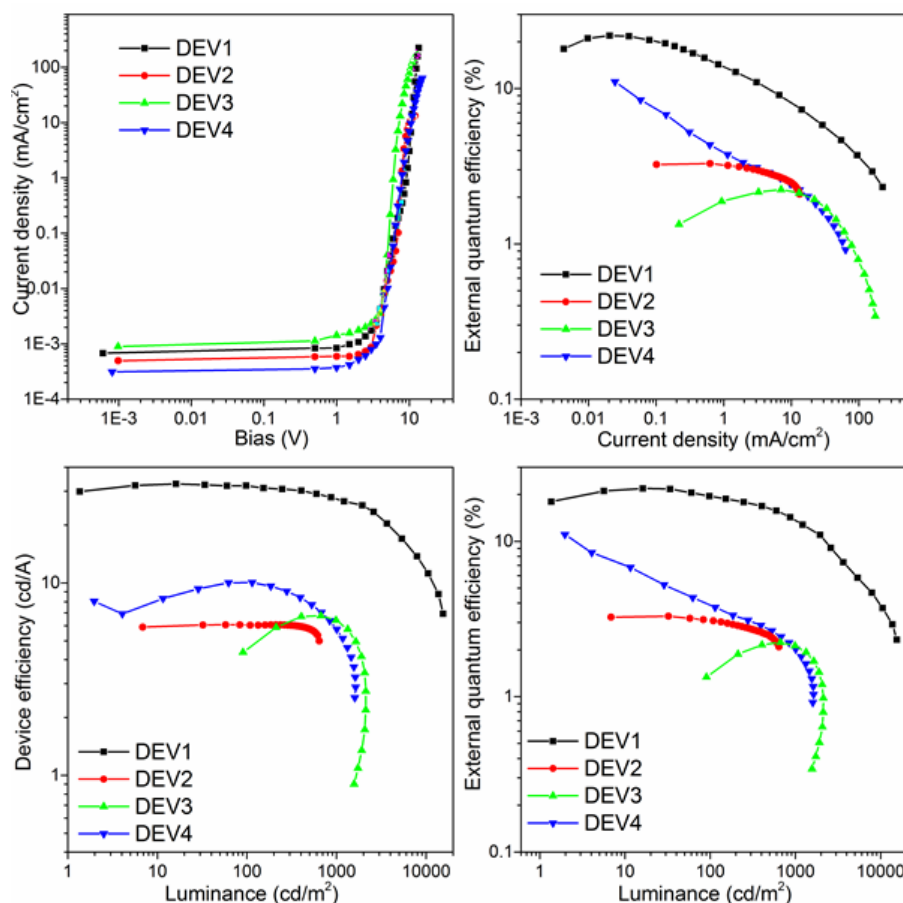


Figure 9- Characteristic of working OLED devices. a) Current density vs. bias, b) EQE vs. current density, c) Device efficiency vs. Luminance, d) EQE vs. Luminance.

3. Summary and conclusions.

In conclusion, the photophysics of TADF in PTZ-DBTO2 was investigated in detail. PTZ-DBTO2 shows very pronounced TADF. The nearly perpendicular arrangement between the D and A units, and the energy alignment of the CT manifold with the local triplet excited state in PTZ-DBTO2 result in very small singlet-triplet splitting and enhanced spin orbit coupling,

which enhances TADF. Devices made of PTZ-DBTO2 show excellent performance with EQE around 19%. We also show efficient TADF and triplet harvesting in tailored organic conjugated polymers based on our PTZ-DBTO2 emitter, and devices were fabricated by solution processing methods. However, solution processed devices of COPO1 and COPO2 showed lower efficiency and are still not able to compete with the performances of current TADF OLEDs based in small molecules. We anticipate that more optimized polymer structures and device fabrication methods will improve device performances of these TADF polymer materials, and we believe that there is now new potential for exploring TADF in solution-processed polymer LEDs, using less costly and more flexible deposition methods, such as spin coating and inkjet printing, for large area deposition.

Experimental Section

Cyclic voltammetry measurements were conducted in 1 mg/ml concentrations of all compounds. Electrochemical studies were conducted in 0.1 M solutions of Bu_4NBF_4 , 99% (Sigma Aldrich) in dichloromethane (DCM) solvent, CHROMASOLV[®], 99.9% (Sigma Aldrich) at room temperature. The electrochemical cell comprised of platinum 1 mm diameter disk as a working electrode, an Ag/AgCl electrode as a reference electrode and a platinum coil as an auxiliary electrode. Cyclic voltammetry measurements were conducted at room temperature at a potential rate of 50 mV/s and were calibrated against a ferrocene/ferrocenium redox couple.

Solution measurements used concentrations in the 10^{-5} – 10^{-4} M range, and samples were degassed using 5 freeze / thaw cycles. PTZ-DBTO2 films in zeonex were prepared by spin coating with PTZ-DBTO2:zeonex ratio of (1:20 w/w). COPO1 and COPO2 films using pristine polymers were prepared by spin-coating from DCM solutions with 10 mg/ml. Absorption and emission spectra were collected using a UV-3600 double beam spectrophotometer (Shimadzu), and a Fluorolog fluorescence spectrometer (Jobin Yvon).

Phosphorescence, prompt fluorescence (PF), and delayed emission (DF) spectra and decays were recorded using nanosecond gated luminescence and lifetime measurements (from 400 ps to 1 s) with either a high energy pulsed Nd:YAG laser emitting at 355 nm (EKSPLA) or a N2 laser emitting at 337 nm. Emission was focused onto a spectrograph and detected on a sensitive gated iCCD camera (Stanford Computer Optics) having sub-nanosecond resolution. PF/DF time resolved measurements were performed by exponentially increasing the gate and delay times.

All organic evaporated compounds were purified by a Creaphys organic sublimation system, NPB - *N,N'*-Di-1-naphthyl-*N,N'*-diphenylbenzidine (TCI-Europe), TPBi - 2,2',2''-(1,3,5-benzenetriyl)-tris(1-phenyl-1*H*-benzimidazole) (LUMTEC), LiF (99.995%, Sigma Aldrich), Aluminium wire (99.9995%, Alfa Aesar).

OLED devices were fabricated using pre-cleaned ITO (Indium-Tin Oxide) coated glass substrates purchased from Ossila with a sheet resistance of 20 Ω/cm^2 and an ITO thickness of 100 nm. The formed OLED devices had a pixel size of 2 mm by 1.5 mm. The small molecule and cathode layers were thermally evaporated using the Kurt J. Lesker Spectros II deposition apparatus at 10^{-6} mbar. All organic materials and aluminum were deposited at a rate of 1 $\text{\AA}\text{s}^{-1}$ and between 0.1 – 2 A/s for coevaporated layers. The LiF layer was deposited at 0.2 $\text{\AA}\text{s}^{-1}$.

References:

¹ (a) H. Uoyama, K. Goushi, K. Shizu, H. Nomura, C. Adachi, *Nature* **2012**, *492*, 234; (b) Y. Tao, K. Yuan, T. Chen, P. Xu, H. Li, R. Chen, C. Zheng, L. Zhang, W. Huang, *Adv. Mater.* **2014**, *26*, 7931. (c) K. Goushi, K. Yoshida, K. Sato, C. Adachi, *Nature Photon.* **2012**, *6*, 253. (d) Q. Zhang, J. Li, K. Shizu, S. Huang, S. Hirata, H. Miyazaki, C. Adachi, *J. Am. Chem. Soc.* **2012**, *134*, 14706.

² C.A. Parker, C.G. Hatchard, *Trans. Faraday Soc.* **1961**, *57*, 1894.

³ M. A. Baldo, D. F. O'Brien, Y. You, A. Shoustikov, S. Sibley, M. E. Thompson, S. R. Forrest, *Nature* **1998**, *395*, 151.

⁴ S. Schmidbauer, A. Hohenleutner, B. König, *Adv. Mater.* **2013**, *25*, 2114.

⁵ X. Xiong, F. Song, J. Wang, Y. Zhang, Y. Xue, L. Sun, N. Jiang, P. Gao, L. Tian, X. Peng, *J. Am. Chem. Soc.* **2014**, *136*, 9590.

- ⁶ (a) M. N. Berberan-Santos, J. M. M. Garcia, *J. Am. Chem. Soc.* **1996**, *118*, 9391. (b) C. Baleizão, M. N. Berberan-Santos, *J. Chem. Phys.* **2007**, *126*, 204510.
- ⁷ (a) C. Adachi, *Jpn. J. Appl. Phys.* **2014**, *53*, 060101. (b) A. Endo, K. Sato, K. Yoshimura, T. Kai, A. Kawada, H. Miyazaki, C. Adachi, *Appl. Phys. Lett.* **2011**, *98*, 083302.
- ⁸ K. Shizu, H. Tanaka, M. Uejima, T. Sato, K. Tanaka, H. Kaji, C. Adachi, *J. Phys. Chem. C* **2015**, *119*, 1291.
- ⁹ Q. Zhang, H. Kuwabara, W. J. Potscavage, Jr., S. Huang, Y. Hatae, T. Shibata, C. Adachi, *J. Am. Chem. Soc.* **2014**, *136*, 18070.
- ¹⁰ I. R. Gould, J. A. Boiani, E. B. Gaillard, J. L. Goodman, *J. Phys. Chem. A* **2003**, *107*, 3515.
- ¹¹ B. T. Lim, S. Okajima, A. K. Chandra, E. C. Lim, *Chem. Phys. Lett.*, **1981**, *79*, 22.
- ¹² S. R. Forrest, *Nature* **2004**, *428*, 911.
- ¹³ Y. J. Cho, K. S. Yook, J. Y. Lee, *Adv. Mater.* **2014**, *26*, 6642.
- ¹⁴ C. Rothe, A. P. Monkman, *J. Chem. Phys.* **2005**, *123*, 244904.
- ¹⁵ V. Jankus, P. Data, D. Graves, C. McGuinness, J. Santos, M. R. Bryce, F. B. Dias, A. P. Monkman, *Adv. Funct. Mater.* **2014**, *24*, 6178.
- ¹⁶ G. Méhes, K. Goushi, W. J. Potscavage Jr., C. Adachi, *Organic Electronics* **2014**, *15*, 2027.
- ¹⁷ Q. Zhang, D. Tsang, H. Kuwabara, Y. Hatae, B. Li, T. Takashi, S. Y. Lee, T. Yasuda, C. Adachi, *Adv. Mater.* **2015**, *27*, 2096.
- ¹⁸ K. Albrecht, K. Matsuoka, K. Fujita, K. Yamamoto, *Angew. Chem. Int. Ed.* **2015**, *54*, 5677.
- ¹⁹ A. E. Nikolaenko, M. Cass, F. Bourcet, D. Mohamad, M. Roberts, *Adv. Mater.* **2015**. DOI: 10.1002/adma.201501090
- ²⁰ F. B. Dias, K. N. Bourdakos, V. Jankus, K. C. Moss, K. T. Kamtekar, V. Bhalla, J. Santos, M. R. Bryce, A. P. Monkman, *Adv. Mater.* **2013**, *25*, 3707.
- ²¹ F. B. Dias, *Phil. Trans. R. Soc. A* **2014**, *373*, 0447.
- ²² Grabowski, *Chem. Rev.* **2003**, *103*, 3899.
- ²³ H. V. Willigen, G. Jones II, M. S. Farabat, *J. Phys. Chem.* **1996**, *100*, 3312.
- ²⁴ Z. E. X. Dance, S. M. Mickley, T. M. Wilson, A. B. Ricks, A. M. Scott, M. A. Ratner, M. R. Wasielewski, *J. Phys. Chem. A* **2008**, *112*, 4194.
- ²⁵ A. M. Scott, M. R. Wasielewski, *J. Am. Chem. Soc.* **2011**, *133*, 3005.
- ²⁶ T. Ogiwara, Y. Wakukawa, T. Ikoma, *J. Phys. Chem. A* **2015**, *119*, 3415.
- ²⁷ A. P. Monkman, H. D. Burrows, I. Hamblett, S. Navaratnam, *Chem. Phys. Lett.* **2001**, *340*, 467.

Supporting Information

Supporting Information is available from the Wiley Online Library or from the author.

Acknowledgements

R.S.N. thanks the financial support from CAPES Foundation, Ministry of Education-Brazil. Grant BEX9474-13-7. Z. R. thanks the China Scholarship Council for funding a visit to Durham University. [†]R.S.N. and Z.R. contributed equally to this work. P. D. acknowledges support from the Mobility Plus project from the Polish Ministry of Science and Higher Education

Received: ((will be filled in by the editorial staff))

Revised: ((will be filled in by the editorial staff))

Published online: ((will be filled in by the editorial staff))

The Photophysics of an electron donor-acceptor molecule showing efficient TADF is studied in detail. Evidence is obtained to show that the energy ordering of the CT and local triplet excited states is crucial to maximize the TADF efficiency. The same DA TADF emitter is then used to design two polymers showing TADF in their pristine films. These results open a new avenue for the design of new TADF emitters and exploring TADF in solution-processed polymer light emitting diodes.

Keyword: TADF; Polymers, OLEDs, PLEDs

Roberto S. Nobuyasu[†], Zhongjie Ren[†], Gareth C. Griffiths, Andrei S. Batsanov, Przemyslaw Data, Shouke Yan, Andrew P. Monkman, Martin R. Bryce, and Fernando B. Dias^{*}

Rational Design of TADF Polymers using a DA Monomer with Enhanced TADF Efficiency induced by the Energy Alignment of Charge Transfer and Local Triplet Excited States.

ToC figure

